Stem Cell Reports
Report
OPEN ACCESS

Tissue-Engineered Vascular Rings from Human iPSC-Derived Smooth Muscle Cells

Biraja C. Dash,[1,2,3] Karen Levi,[4] Jonas Schwan,[5] Jiesi Luo,[1,2] Oscar Bartulos,[1,2] Hongwei Wu,[1,2,6] Caihong Qiu,[2] Ting Yi,[1,2] Yongming Ren,[1,2] Stuart Campbell,[5] Marsha W. Rolle,[4] and Yibing Qyang[1,2,7,8,*]
[1]Section of Cardiovascular Medicine, Department of Internal Medicine, Yale Cardiovascular Research Center, Yale School of Medicine, New Haven, CT 06511, USA
[2]Yale Stem Cell Center, Yale University, New Haven, CT 06510, USA
[3]Department of Surgery (Plastic), Yale University, New Haven, CT 06520, USA
[4]Department of Biomedical Engineering, Worcester Polytechnic Institute, Worcester, MA 01609, USA
[5]Department of Biomedical Engineering, Yale University, New Haven, CT 06510, USA
[6]Department of Orthopedics, Hunan Cancer Hospital and The Affiliated Cancer Hospital of Xiangya School of Medicine, Central South University, Changsha, Hunan 410011, China
[7]Vascular Biology and Therapeutics Program, Yale School of Medicine, New Haven, CT 06510, USA
[8]Department of Pathology, Yale University, New Haven, CT 06510, USA
*Correspondence: yibing.qyang@yale.edu
http://dx.doi.org/10.1016/j.stemcr.2016.05.004

SUMMARY

There is an urgent need for an efficient approach to obtain a large-scale and renewable source of functional human vascular smooth muscle cells (VSMCs) to establish robust, patient-specific tissue model systems for studying the pathogenesis of vascular disease, and for developing novel therapeutic interventions. Here, we have derived a large quantity of highly enriched functional VSMCs from human induced pluripotent stem cells (hiPSC-VSMCs). Furthermore, we have engineered 3D tissue rings from hiPSC-VSMCs using a facile one-step cellular self-assembly approach. The tissue rings are mechanically robust and can be used for vascular tissue engineering and disease modeling of supravalvular aortic stenosis syndrome. Our method may serve as a model system, extendable to study other vascular proliferative diseases for drug screening. Thus, this report describes an exciting platform technology with broad utility for manufacturing cell-based tissues and materials for various biomedical applications.

INTRODUCTION

Dysfunction of vascular smooth muscle cells (VSMCs) frequently leads to vascular disease and represents one of the largest causes of mortality (Michel et al., 2012). Animal models and primary VSMC culture-based approaches have been informative in unraveling disease mechanisms (Chang et al., 2014; Zaragoza et al., 2011). However, there are significant barriers to progress in the field of basic and translational research of vascular disease due to (1) significant differences in vascular physiology between mice and humans; (2) limited access to patient VSMCs; and (3) lack of patient-specific, 3D tissue models that provide a closer approximation of the in vivo environment. It is also worth noting that the lack of robust human cell-based disease models has contributed to the failure of a number of clinical trials that were largely based upon animal studies (Rubin, 2008). Thus, it is necessary to obtain an abundant and renewable source of functional human VSMCs and to establish robust, human tissue model systems for studying the pathogenesis of vascular disease, and for developing novel therapeutic interventions.

Induced pluripotent stem cell (iPSC) technology holds great promise for future autologous cellular therapies for vascular diseases (Tavernier et al., 2013). However, a major concern is the availability of approaches to differentiate iPSCs into large quantities of functional VSMCs for research and therapeutic applications (Dash et al., 2015). VSMCs have been previously derived from human iPSCs (hiPSCs) with different approaches (Bajpai et al., 2012; Cheung et al., 2012; Lee et al., 2009; Patsch et al., 2015; Wanjare et al., 2013). However, an efficient, large-scale production of highly enriched, functional hiPSC-VSMCs suitable for vascular tissue engineering still awaits to be established. In this study, hiPSCs from fibroblast cells were generated using Sendai virus (SeV) vectors. We also derived a large quantity of highly enriched, functional hiPSC-VSMCs based on a robust embryoid body (EB) approach. In addition, we used a scaffold-free, self-assembly approach to engineer robust 3D model vascular tissue constructs from both normal and disease-specific human VSMCs.

RESULTS

Integration-free hiPSC Generation and Characterization

Integration-free hiPSCs were generated with neonatal skin fibroblast cells derived from a healthy female donor using SeV particles that encode OCT3/4, KLF4, SOX2, and c-MYC genes. The selected hiPSC clones exhibited a

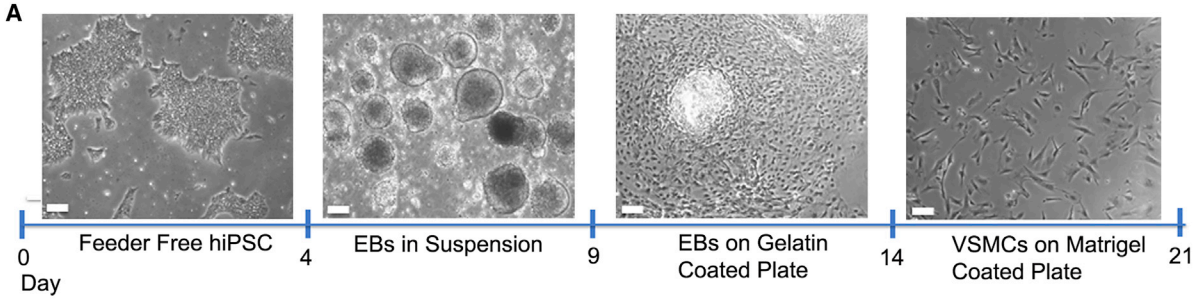

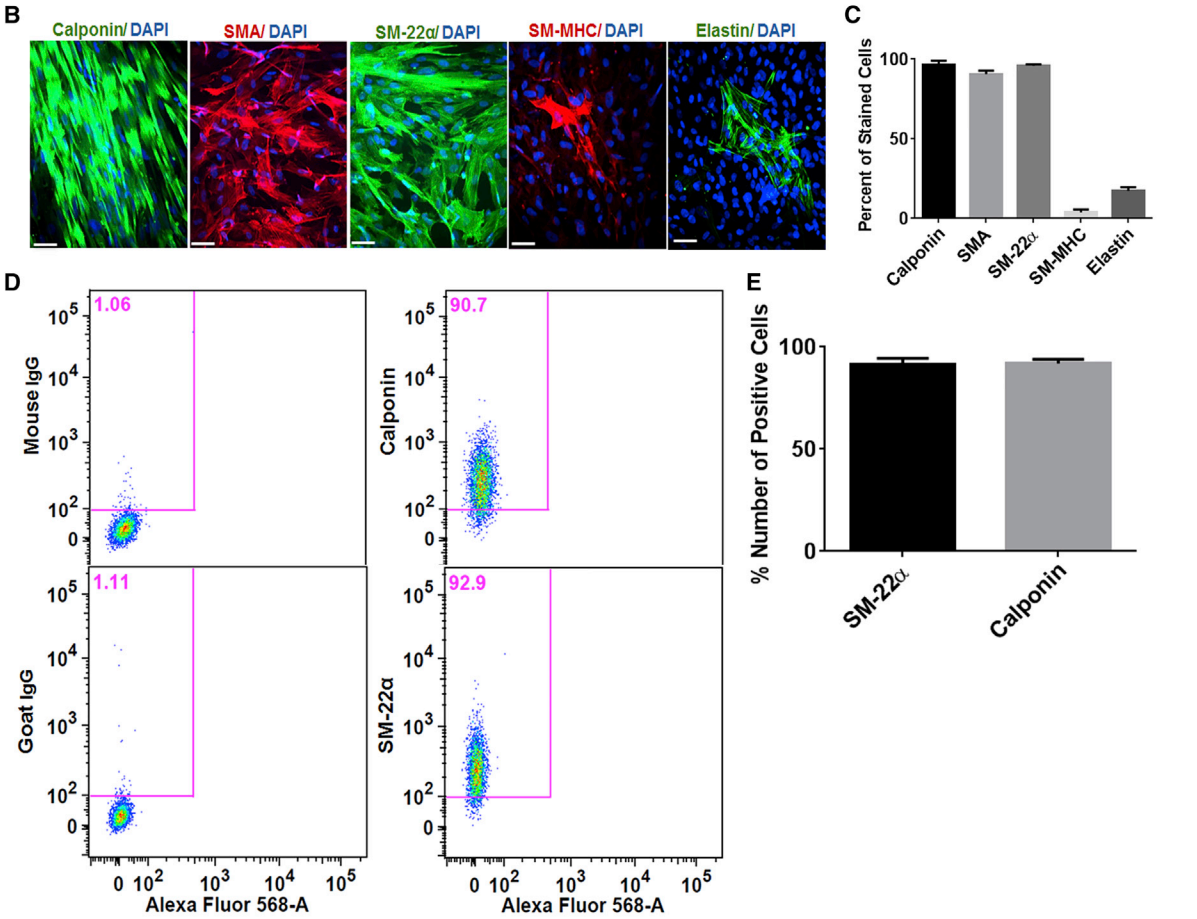

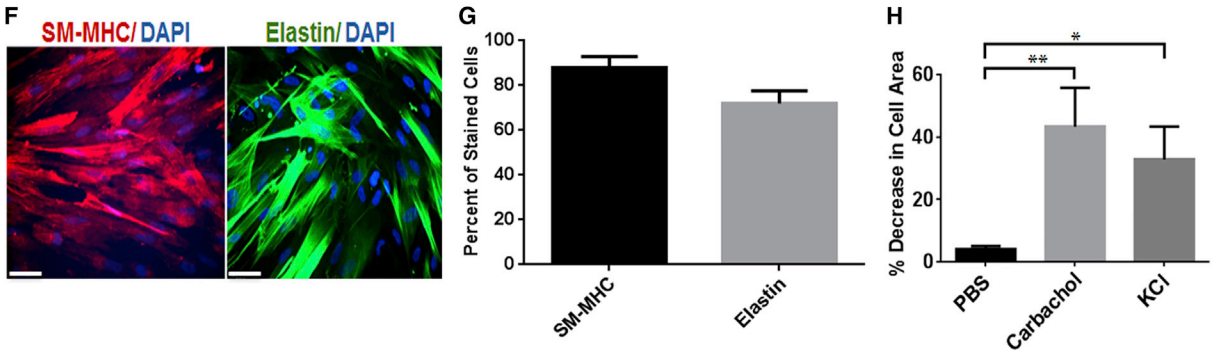

(legend on next page)

typical compact phenotype indistinguishable from human embryonic stem cells and were positive for pluripotency markers, including OCT4, NANOG, SSEA-4, and Tra-1-60 (Figure S1A). G-band staining for karyotype analysis indicated that hiPSC clones were karyotypically normal (Figure S1B) and were also found to be free of SeV vectors (typically after 15 passages), as shown by RT-PCR (Figure S1C). The hiPSCs formed teratomas and revealed the presence of representative tissues that originated from the three embryonic germ layers (Figure S1D), including the gastrointestinal epithelium (endoderm), pigmented epithelium (ectoderm), and hyaline cartilage (mesoderm). Integration-free hiPSC clones (named as Y6) were then continuously propagated and used for differentiation and characterization of VSMCs.

Derivation of Large Quantities of Pure, Functional VSMCs from hiPSCs

An EB differentiation protocol was used to induce hiPSC differentiation toward a VSMC lineage. The entire differentiation procedure (shown schematically in Figure 1A) requires 21 days starting from hiPSC culture. Since the derivation of VSMCs from hiPSCs using the earlier reported EB method (Xie et al., 2007) was inefficient and could not generate large numbers of VSMCs for therapeutic studies, significant modifications were made to the existing approach, where 80% confluent hiPSCs grown under feeder-free culture were used to make EBs. Moreover, pure mTeSR1 (iPSC self-renewal media) and 25% mTeSR1-containing EB differentiation media was used to culture day 1 and day 2 EBs, respectively. These two modifications resulted in the production of much healthier EBs and an abundance of highly enriched VSMCs. After 7 days of culture in SmGM-2 (a commercially available medium optimized for VSMC growth), 96.25% ± 2.70%, 90.59% ± 2.20%, and 95.81% ± 0.99% of VSMCs expressed calponin, α-smooth muscle actin (SMA), and SM-22α, respectively (Figures 1B, 1C, and S2A). In addition, fluorescence-activated cell sorting (FACS) analysis showed 91.66% ± 2.78% of hiPSC-VSMCs positive for SM-22α and 91.86% ± 2.05% of hiPSC-VSMCs positive for calponin (Figures 1D, 1E, and S2B). The expression of mature VSMC markers such as smooth muscle myosin heavy chain (SM-MHC) and elastin in hiPSC-VSMCs increased from 3.86% ± 1.80% and 17.32% ± 2.30%, when cultured in the SmGM-2 growth medium (Figures 1B and 1C), to 87.45% ± 7.10% and 74.65% ± 4.60%, respectively, when switched to a maturation medium containing 0.5% fetal bovine serum (FBS) and 1 ng/ml transforming growth factor β1 (TGF-β1) for 10 days (Figures 1F and 1G). The expression level of the VSMC mature markers elastin and SM-MHC in the maturation medium was further validated by examining the gene-expression level of elastin and by FACS analysis of SM-MHC-positive cells (Figures S2C and S2D). A similar pattern of increase in elastin and SM-MHC was seen after culturing VSMCs in the maturation medium. The elastin gene-expression level increased 3-fold in the maturation medium compared with that in the growth-promoting SmGM-2 medium (Figure S2C). Likewise, an increase in the SM-MHC-positive cells was seen when the VSMCs were cultured in the maturation medium. The SM-MHC-positive cells increased from 3.24% ± 2.76% in SmGM-2 medium to 79.07% ± 5.89% in the maturation medium (Figure S2D). In addition, hiPSC-VSMCs showed contractility in response to agonists such as carbachol and KCl, measured by quantifying percent decrease in the cell area. The treatments with carbachol and KCl induced a 43.31% ± 12.43% and 32.83% ± 10.47% decrease in the cell area, respectively, compared with PBS control (Figures 1H and S3).

The scalability (Figure 2A) and efficiency of the protocol were tested in three different hiPSC lines (all from healthy

Figure 1. Characterization of hiPSC-VSMCs

(A) Schematic diagram along with representative images showing the hiPSC-VSMC differentiation method. Scale bar represents 100 μm.

(B) Immunofluorescence images of cells stained with smooth muscle cell markers calponin, SMA, SM-22α, SM-MHC, and elastin in hiPSC-VSMCs cultured in SmGM-2 medium for 7 days. Red (SMA and SM-MHC), green (SM-22α, calponin, and elastin), and blue (nuclei). Scale bar represents 50 μm. The Y6 hiPSC line was used to derive VSMCs.

(C) Graph showing percentage of VSMCs positive for calponin, SMA, SM-22α, SM-MHC, and elastin in three independent experiments (mean ± SD; n = 3 independent experiments).

(D) Fluorescence-activated cell sorting (FACS) data showing VSMC purity, quantified with smooth muscle cell-specific markers SM-22α and calponin. Goat and mouse IgGs were used as negative controls for SM-22α and calponin, respectively.

(E) Graph showing percentage of VSMCs positive for SM-22α and calponin in three independent FACS experiments (mean ± SD; n = 3 independent experiments).

(F) Immunofluorescence images of hiPSC-VSMCs cultured in a medium containing 0.5% FBS and 1 ng/ml TGF-β1 for 10 days and stained for SM-MHC and elastin. Red (SM-MHC), green (elastin), and blue (nuclei). Scale bar represents 50 μm.

(G) Graph showing percentage of VSMCs positive for SM-MHC and elastin in three independent experiments.

(H) Graph showing percent decrease in cell area in response to agonists KCl and carbachol. Unpaired Student's t test was performed to determine the statistical difference between different groups (mean ± SD; n = 3 independent experiments, *p < 0.05, **p < 0.01). See Figures S1–S3 and Tables S1 and S2 for additional controls and supporting information.

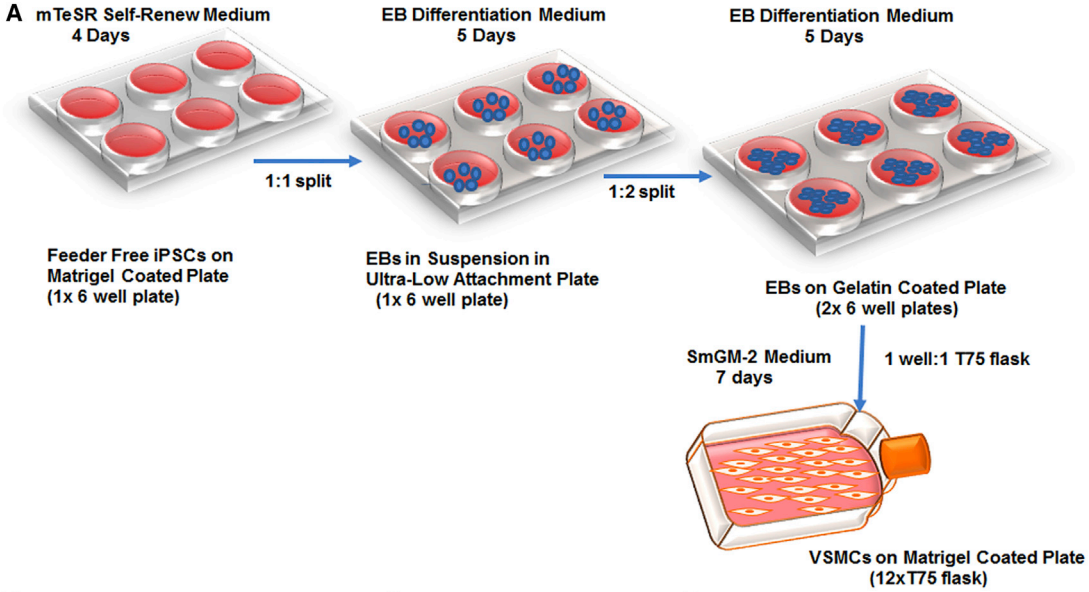

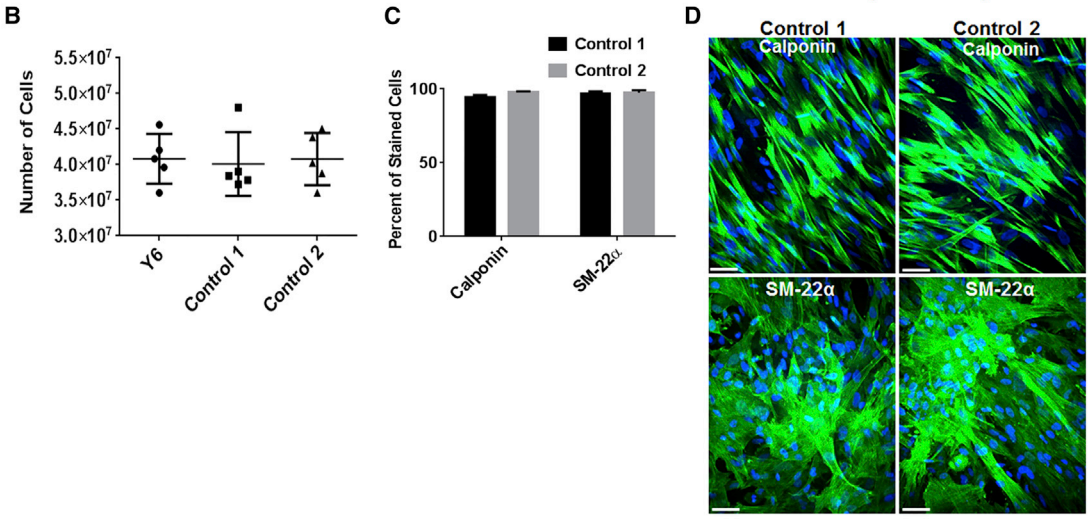

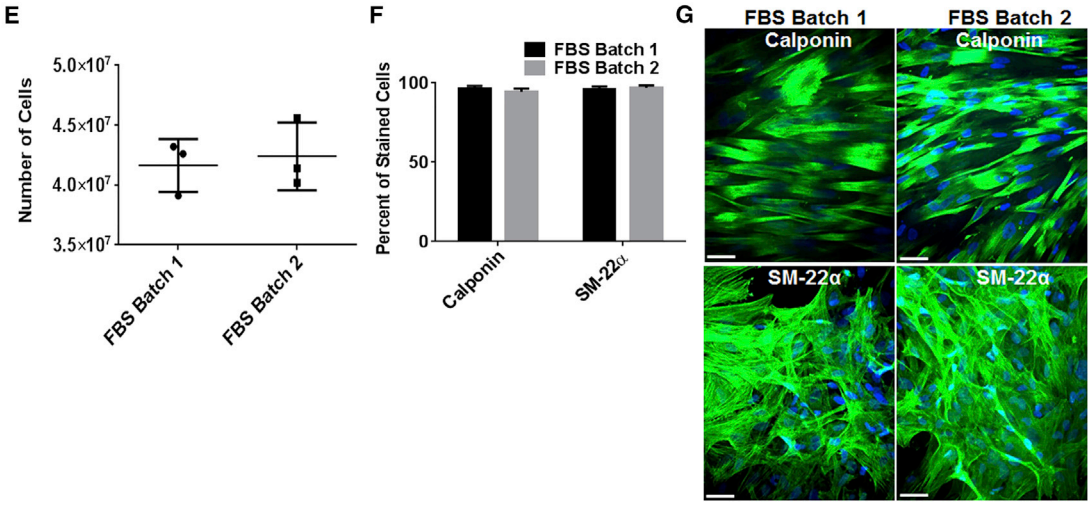

(legend on next page)

subjects): Y6 (established in this study; Figure S1), control 1 (Ge et al., 2012), and control 2 (Chen et al., 2013), and two different batches of FBS (Figures 2B and 2E). The protocol consistently generated about 40 × 10^6 hiPSC-VSMCs for all three hiPSC lines and both batches of FBS (Figures 2B and 2E). In addition, purities of these hiPSC-VSMCs were quantified using SM-22α and calponin. Control 1 and control 2 hiPSC-VSMCs were 94.46% ± 1.30% and 97.96% ± 0.40% positive for calponin and 96.85% ± 1.50% and 97.57% ± 1.50% for SM-22α, respectively (Figures 2C and 2D). Similarly, FBS batch 1- and 2-derived hiPSC-VSMCs were 96.27% ± 1.90% and 94.36% ± 2.00% positive for calponin and 96.11% ± 1.7% and 96.93% ± 1.4% positive for SM-22α, respectively (Figures 2F and 2G).

VSMCs from different vessels have different embryological origin, and these different VSMC subtypes can be distinguished by their distinct in vitro proliferative responses to angiotensin II, TGF-β1, and serum (Cheung et al., 2012). Cell-proliferation assays were performed to determine the hiPSC-VSMC subtype (Figures S2E–S2G). MTT assay after 3 days in culture showed an increased response of hiPSC-VSMCs to serum (Figure S2E), but not to TGF-β1 and angiotensin II. A similar response of hiPSC-VSMCs to serum was observed with cell counting (Figure S2F) and cell-cycle analysis (percentage of proliferating cells in S and G2-M) (Figure S2G). These results are consistent with the notion that hiPSC-VSMCs may contain a significant population of lateral plate mesoderm-derived VSMCs that show a proliferative response to serum but not to TGF-β1 or angiotensin II.

We also found that hiPSC-VSMCs cultured for 7 days in a ring tissue culture medium with 20% FBS, growth factors (platelet-derived growth factor-BB [PDGF-BB] and TGF-β1), and other supplements ($CuSO_4$, proline, glycine, alanine, and ascorbic acid) proliferated (Figure S4A) and were able to produce extracellular matrix such as type I collagen (Figure S4B). This ring culture medium was subsequently used to culture 3D hiPSC-VSMC tissue ring constructs as described below.

Robust Tissue Ring Fabrication and Disease Modeling

Previous studies have reported the use of VSMCs derived from hiPSCs as 2D cell culture models to study vascular disease mechanisms (Ge et al., 2012). However, 3D engineered tissue models may more closely mimic in vivo vascular physiology, as cell-cell and cell-matrix interactions are markedly different between the in vivo environment and in vitro 2D cell culture. So far, only a few studies have reported using stem cell-derived VSMCs for tissue engineering applications using natural or synthetic scaffold materials (Bajpai et al., 2012; Karamariti et al., 2013; Sundaram et al., 2014; Wang et al., 2014). However, none have reported using a scaffold-free approach to create 3D engineered vascular tissues. In this study, we employed a scaffold-free cellular self-assembly approach (Gwyther et al., 2011b) to generate hiPSC-VSMC tissue rings. Briefly, hiPSC-VSMCs cultured in SmGM-2 were harvested and seeded into ring-shaped agarose wells (Figure 3A). hiPSC-VSMCs aggregated and contracted around the center posts of the non-adhesive agarose wells and successfully formed tissue rings within 1 day of seeding.

In preliminary studies, we found that hiPSC-VSMC rings cultured in SmGM-2 continued to contract in the agarose wells, resulting in thinning and failure between 4 and 7 days of culture (Figure S4C). Subsequently, hiPSC-VSMCs were seeded in SmGM-2, then switched to a ring culture medium with 20% FBS, PDGF-BB, TGF-β1, and other collagen-promoting supplements 24 hr after cell seeding. The rings cultured in ring culture medium were stable and did not show appreciable contraction. hiPSC-VSMC rings were cultivated in the ring culture medium for 14–17 days before harvesting for histology and mechanical testing. Representative photographs of tissue rings derived from Y6 hiPSC-VSMCs after 14 days in culture are shown in Figure 3A. Hematoxylin and eosin staining showed highly cellularized tissue rings (Figure 3B). Masson's trichrome staining showed an abundance of collagen in the extracellular matrix of these tissue rings (Figure 3B), which was also shown by immunostaining for type I collagen (Figure S4D). Immunohistochemical analyses also showed

Figure 2. Larger-Scale VSMC Derivation from hiPSCs

(A) Schematic diagram showing the procedure for derivation of hiPSC-VSMCs with high purity.

(B–D) Characterization of hiPSC-VSMCs derived from two other hiPSC lines, control 1 and control 2. Control 1 and control 2 hiPSC-VSMC purity was quantified using calponin and SM-22α markers. (B) Resulting cell numbers from replicate derivations of VSMCs from Y6, control 1, and control 2 hiPSCs after 17 days of differentiation (n = 3 independent experiments). (C) Graph showing percentage of VSMCs positive for calponin or SM-22α in three independent experiments. (D) Representative immunofluorescence images of cells stained with calponin and SM-22α. Green stains for both calponin and SM-22. Blue stains for nuclei. Scale bar represents 50 μm.

(E–G) Characterization of Y6-VSMCs derived using two different batches of FBS. (E) Quantification of cell numbers generated from hiPSC-VSMC derivations using two different batches of serum (n = 3 independent experiments). (F) Graph showing percentage of positive VSMCs for calponin and SM-22α in three independent experiments. (G) Immunofluorescence images of cells stained with calponin and SM-22α. Green stains for both calponin and SM-22α. Blue stains for nuclei. Scale bar represents 50 μm. The data are represented as means ± SD. Also see Figure S2.

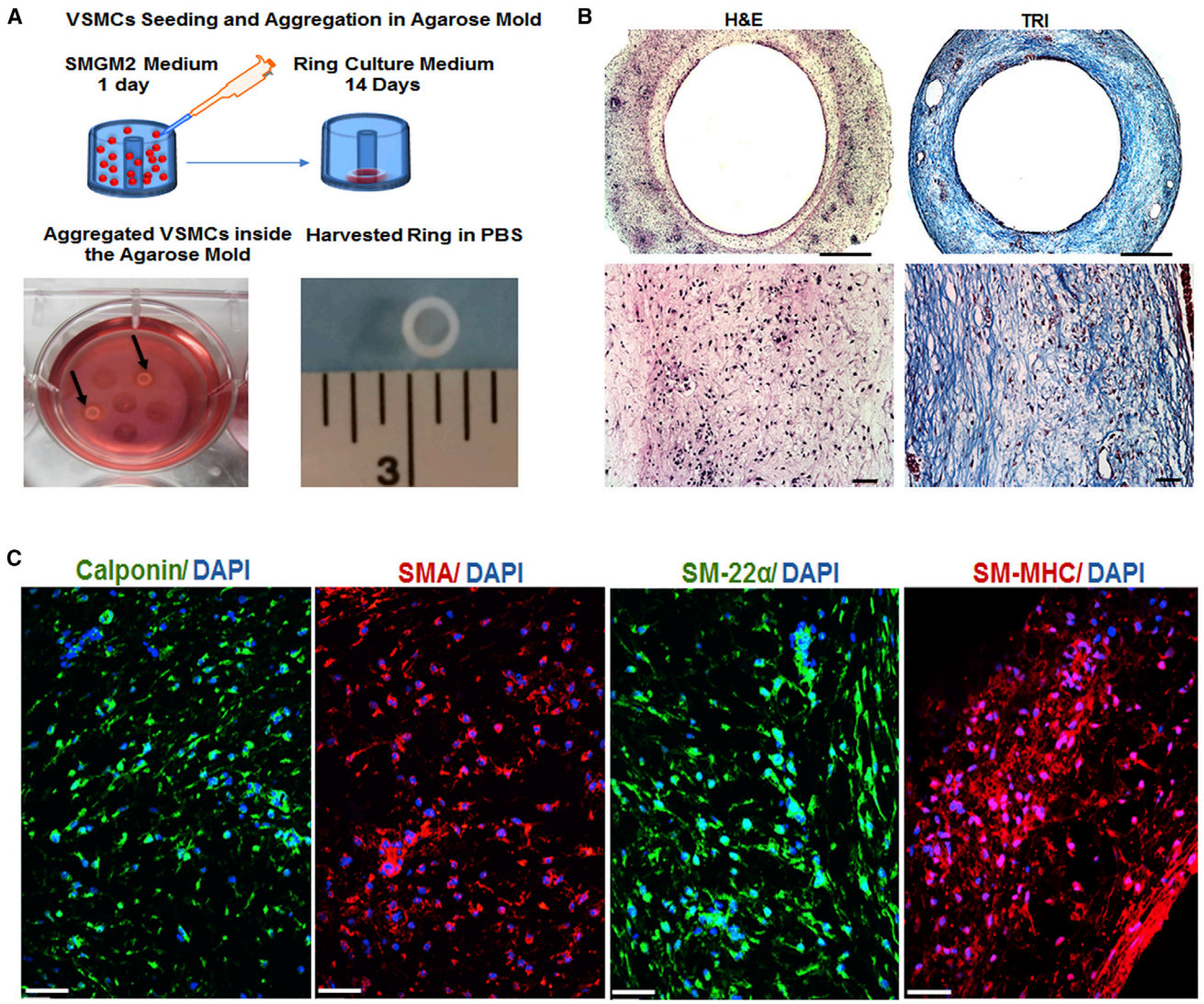

Figure 3. Tissue Ring Fabrication and Characterization Using Y6 hiPSC-VSMCs

(A) Schematic showing tissue ring fabrication by cellular self-assembly, and photographs of tissue rings in the agarose mold (black arrow) and a harvested tissue ring.

(B) Histochemical analysis of the tissue rings with H&E (left) and Masson's trichrome (TRI: right) staining. The pink in H&E staining represents cytoplasm and the blue in Masson's trichrome represents collagen. The dark purple in both H&E and Masson's trichrome staining represents nuclei. Scale bars represent 500 and 100 μm, respectively, for lower and higher magnification images.

(C) Immunofluorescence analysis of calponin (green), SMA (red), SM-22α (green), and SM-MHC (red) present in the tissue rings after 14 days in culture. Blue stains for nuclei. Scale bar represents 50 μm. Also see Figure S4.

that hiPSC-VSMCs within tissue rings cultured for 14 days were positive for calponin, SMA, SM-22α, and SM-MHC (Figure 3C), suggesting that the cells retained a VSMC phenotype during culture as self-assembled, high-density VSMC tissue rings.

Tissue rings from two independent batches were mechanically strong when harvested after 14 or 17 days in culture (Figure 4). Stress-strain plots were generated from each of the tissue ring samples tested (representative plot shown in Figure 4A) and used to calculate ultimate tensile strength (UTS) and maximum tangent modulus. Mechanical testing data for both batches of Y6 hiPSC-VSMC rings are summarized in Figure 4B. The average thickness of the 2 mm inner diameter tissue rings was 0.84–0.87 mm after 14–17 days in culture. Overall, hiPSC-VSMCs exhibited greater UTS than 14-day-old rat aortic or human coronary artery SMC rings (2 mm, inner diameter) reported previously (Gwyther et al., 2011a, 2011b). In addition, the contractile response

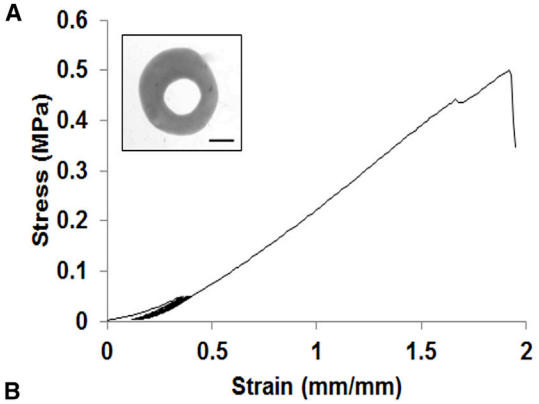

B

Sample Size (n =)	Culture Duration (days)	Ring Thickness (mm)	UTS (MPa)	MTM (MPa)	Max Load (N)	Max Extension (mm)
7	14	0.87 ± 0.05	0.473 ± 0.134	0.442 ± 0.156	0.555 ± 0.140	2.49 ± 0.47
3	17	0.84 ± 0.08	0.366 ± 0.066	0.138 ± 0.021	0.412 ± 0.121	5.84 ± 1.41

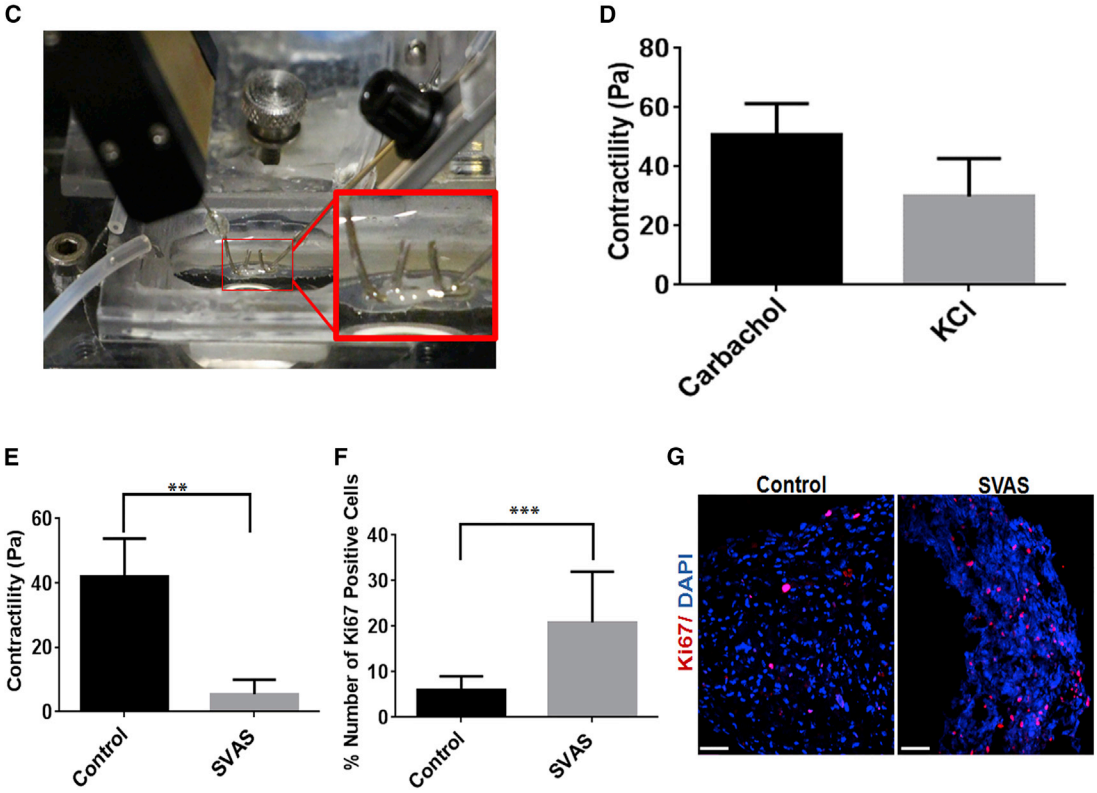

Figure 4. Mechanical and Functional Characterization of hiPSC-VSMC Rings

(A) Representative stress-strain curve of a 14-day-old tissue ring (inset, digital image of ring used to measure thickness and calculate cross-sectional area; scale = 1 mm).

(B) Results of mechanical tests from two independent batches of hiPSC-VSMC tissue rings (mean ± SD; n = 7 and 3 independent measurements for day 14 and 17, respectively).

(legend continued on next page)

of the hiPSC-VSMC tissue rings in response to agonists, carbachol (1 mM) and KCl (50 mM), was measured (Figures 4C and 4D). The contractility was measured using an instrument with a force transducer, in which a contraction by the rings in response to agonists induces an increase in force (Figure 4C). The contraction was shown as tension (Pascal) by a normalizing force with their respective cross-section areas. The rings showed a contraction of 67.35 ± 22.7 Pa in response to carbachol, whereas the response was 44.44 ± 27.13 Pa for KCl (Figure 4D).

Furthermore, we tested whether the tissue ring system could be used to model vascular proliferative diseases such as supravalvular aortic stenosis (SVAS) syndrome. In SVAS, hyperproliferation of VSMCs leads to blockage of the aorta and arteries. Highly enriched VSMCs were derived from control and SVAS (Ge et al., 2012) hiPSCs (Figure S4E). Tissue rings were successfully fabricated from these hiPSC-VSMCs. The tissue rings were characterized for their difference in contractility and percent of proliferating cells using Ki67 immunostaining. The ring contractility study showed control rings with a contraction of 42.01 ± 11.77 Pa in response to carbachol, whereas the response was 5.51 ± 4.51 Pa for SVAS rings (Figure 4E). The percentage of Ki67-positive cells was 6.31% ± 3.16% for control rings and 21.73% ± 11.96% for SVAS rings (Figures 4F and 4G). Immunofluorescence analyses of cultured cells revealed more actin filament bundle formation in the control iPSC-VSMCs than in the SVAS iPSC-VSMCs (Figure S4E), consistent with the results described in our earlier report (Ge et al., 2012). In addition, there was an increased percentage of cells expressing SM-MHC in the control iPSC-VSMCs compared with the SVAS iPSC-VSMCs (Figure S4E).

DISCUSSION

In this study, we generated an abundant and renewable source of functional VSMCs from multiple hiPSC lines. The success of VSMC production appears to be independent of the somatic cell sources (Y6: fibroblasts; control 1, VSMCs; control 2, peripheral blood mononuclear cells) and derivation approaches (Y6 and control 2, non-integrating SeV; control 1, lentiviral) used to generate the hiPSC lines. The feeder-free culture approach resulted in healthier and robust EBs, enabling us to derive ~40 million VSMCs within 21 days of differentiation time from a 6-well plate of hiPSCs. The VSMCs were highly enriched for SM-22α, SMA, and calponin and can further be induced into mature VSMCs expressing SM-MHC and elastin. The VSMC derivation method was found to be efficient with different hiPSC lines and also with different batches of FBS. The hiPSC-VSMCs were functional and responded to chemical stimuli such as carbachol and KCl. We have also investigated different VSMC subtypes using an assay described previously (Cheung et al., 2012). hiPSC-VSMCs showed significant proliferation in response to serum, but only exhibited a modest trend of response upon treatment with TGF-β1 or angiotensin II without reaching statistical significance. These results suggest that hiPSC-VSMCs derived in this study may contain a significant population of VSMCs derived from the lateral plate mesoderm.

We then used a cellular self-assembly approach to create hiPSC-VSMC tissue rings. Histological analysis of 14-day-old rings showed high cellularity and VSMC marker expression, including SMA, SM-22α, calponin, and SM-MHC. Type I collagen was also abundantly found in these tissue rings. hiPSC-VSMC tissue rings are mechanically strong enough to endure physical handling and mechanical testing within 7–14 days of cell seeding. In addition, we measured normal and SVAS hiPSC-VSMC contractility in 3D tissue constructs, suggesting that the ring self-assembly system, coupled with patient-specific VSMCs, can be used to create functional model human vascular tissues. SVAS, an autosomal disease, is caused by loss-of-function mutations in the elastin gene and is characterized by hyperproliferation of VSMCs leading to blockage of the ascending aorta and other arterial vessels (Ge et al., 2012). Patients with Williams-Beuren syndrome (WBS) also display SVAS (Ge et al., 2012). Earlier 2D studies in cell culture (Ge et al., 2012; Kinnear et al., 2013) reveal that SVAS and WBS iPSC-VSMCs are less contractile and more proliferative than control iPSC-VSMCs. We were able to model these two important

(C) Photograph showing VSMC tissue ring hooked on two micromanipulators and immersed in a temperature-controlled perfusion bath containing Tyrode's solution for the contractility assay.

(D) Graph showing change in contractility (Pascal) in response to the agonists KCl and carbachol. PBS was used as negative control.

(E) Graph showing change in contractility (Pascal) of control and SVAS rings in response to carbachol. Unpaired Student's t test was performed to determine statistical difference between different groups (mean ± SD; n = 3 independent experiments, $^{**}p < 0.01$). PBS was used as negative control.

(F) Graph showing percent number of Ki67-positive cells in control and SVAS rings. The data are represented as mean ± SD. Unpaired Student's t test was performed to determine statistical difference between different groups (n = 3 independent experiments, $^{***}p < 0.001$).

(G) Representative immunofluorescence images of control and SVAS rings stained with Ki67. Red (Ki67) and blue (nuclei). Scale bar represents 50 μm. Also see Figure S4.

characteristics of SVAS in the physiologically more relevant 3D tissue rings. The SVAS tissue rings showed significantly less contractility and more proliferative cells than control rings. The lower contractile forces generated by SVAS rings might be due to decreased formation of actin filament bundles and fewer cells expressing SM-MHC in SVAS VSMCs compared with those in control VSMCs.

Primary tissue- or hiPSC-derived VSMCs have been previously used to establish vascular tissue constructs with different scaffold materials, such as polyglycolic acid, fibrin, and poly-L-lactic acid (Bajpai et al., 2012; Niklason et al., 1999; Sundaram et al., 2014; Wang et al., 2010). However, these artificial materials are significantly different from the natural extracellular matrix produced by VSMCs. In contrast, our unique scaffold-free technique has enabled fabrication of patient-specific tissue constructs engineered entirely from human VSMCs and the extracellular matrix they produce. The facile, one-step cell-seeding process results in robust, scaffold-free tissue constructs within a short duration of culture time (less than 2 weeks) without specialized equipment. Finally, these tissue rings may be useful as modular building blocks to generate tubular tissue constructs to be used for vascular grafts (Gwyther et al., 2011a, 2011b), or as model in vitro vascular tissues for drug discovery and to study human disease mechanisms.

In the future, we will fabricate tissue rings from various lineage-specific hiPSC-VSMCs and disease-specific VSMCs for disease modeling and drug screening. Further optimization of the culture conditions such as use of Ficoll, a macromolecular crowder, in the culture medium will be tested in order to enhance the strength of the tissue rings (Zeiger et al., 2012). Finally, our methodology can potentially be extended to fabricate tissue rings from other types of cells derived from patient-specific hiPSCs for the construction of mechanically robust engineered tissues for disease research and treatment.

EXPERIMENTAL PROCEDURES

Animal Studies

Immunodeficient Rag2-/-GammaC-/- mice were used for teratoma assay. All animal studies were approved by the Yale IACUC protocol (2013-11347) and performed in accordance with the NIH guidelines for care and use of laboratory animals.

hiPSC-VSMC Derivation

hiPSC-VSMCs were derived using a modified EB protocol which results in a larger-scale generation of VSMCs at the end of 21 days. A detailed protocol is described in the Supplemental Information.

Tissue Ring Fabrication

Custom agarose molds for tissue ring formation were made as previously described (Gwyther et al., 2011a, 2011b), with minor modifications (Dikina et al., 2015). A detailed protocol is described in the Supplemental Information.

2D and 3D Contractility Study

The 2D SMC contraction study was carried out using hiPSC-VSMCs cultured on tissue culture plastic. KCl (50 mM) and carbachol (1 mM) were used as agonists. Similarly, tissue rings were tested for their contractility in response to carbachol. A detailed protocol can be found in the Supplemental Information.

Tissue Ring Mechanical Testing

Mechanical testing was performed using an uniaxial tensile testing machine (Electropuls E1000, Instron) as previously described (Gwyther et al., 2011b). A detailed protocol can be found in the Supplemental Information.

Statistical Analysis

Statistical analyses were performed using GraphPad Prism 6. One-way ANOVA was used to compare the cell proliferation between different time points, and two-tailed Student's t test was used for pair comparisons.

SUPPLEMENTAL INFORMATION

Supplemental Information includes Supplemental Experimental Procedures, four figures, and two tables and can be found with this article online at http://dx.doi.org/10.1016/j.stemcr.2016.05.004.

AUTHOR CONTRIBUTIONS

B.C.D., M.R., and Y.Q. conceived the study; B.C.D., K.L., J.S., O.B., J.L., H.W., C.Q., and T.Y. performed the research; Y.R. and S.C. contributed analytic tools; B.C.D., K.L., J.S., O.B., C.Q., T.Y., M.R., and Y.Q. analyzed the data; B.C.D. and Y.Q. wrote the manuscript; and K.L. and M.R. edited the manuscript.

ACKNOWLEDGMENTS

We would like to thank Drs Laura Niklason and Liqiong Gui for their timely scientific suggestions and Dr Daniel Greif for his suggestions on the manuscript. This work is supported by NSF DGE-1144804 (K.L. and M.R.), NIH 1K02HL101990-01, 1R01HL116705-01, Connecticut's Regenerative Medicine Research Fund (R.M.R.F.) and 12-SCB-YALE-06 (Y.Q.). Control 2 human iPSC line is a generous gift of Dr I-Ping Chen from the University of Connecticut Health Science Center.

Received: March 4, 2015
Revised: May 8, 2016
Accepted: May 8, 2016
Published: July 12, 2016

REFERENCES

Bajpai, V.K., Mistriotis, P., Loh, Y.H., Daley, G.Q., and Andreadis, S.T. (2012). Functional vascular smooth muscle cells derived from human induced pluripotent stem cells via mesenchymal stem cell intermediates. Cardiovasc. Res. *96*, 391–400.

Chang, S., Song, S., Lee, J., Yoon, J., Park, J., Choi, S., Park, J.K., Choi, K., and Choi, C. (2014). Phenotypic modulation of primary vascular smooth muscle cells by short-term culture on micropatterned substrate. PLoS One *9*, e88089.

Chen, I.P., Fukuda, K., Fusaki, N., Iida, A., Hasegawa, M., Lichtler, A., and Reichenberger, E.J. (2013). Induced pluripotent stem cell reprogramming by integration-free Sendai virus vectors from peripheral blood of patients with craniometaphyseal dysplasia. Cell Reprogram. *15*, 503–513.

Cheung, C., Bernardo, A.S., Trotter, M.W., Pedersen, R.A., and Sinha, S. (2012). Generation of human vascular smooth muscle subtypes provides insight into embryological origin-dependent disease susceptibility. Nat. Biotechnol. *30*, 165–173.

Dash, B.C., Jiang, Z., Suh, C., and Qyang, Y. (2015). Induced pluripotent stem cell-derived vascular smooth muscle cells: methods and application. Biochem. J. *465*, 185–194.

Dikina, A.D., Strobel, H.A., Lai, B.P., Rolle, M.W., and Alsberg, E. (2015). Engineered cartilaginous tubes for tracheal tissue replacement via self-assembly and fusion of human mesenchymal stem cell constructs. Biomaterials *52*, 452–462.

Ge, X., Ren, Y., Bartulos, O., Lee, M.Y., Yue, Z., Kim, K.Y., Li, W., Amos, P.J., Bozkulak, E.C., Iyer, A., et al. (2012). Modeling supravalvular aortic stenosis syndrome with human induced pluripotent stem cells. Circulation *126*, 1695–1704.

Gwyther, T.A., Hu, J.Z., Billiar, K.L., and Rolle, M.W. (2011a). Directed cellular self-assembly to fabricate cell-derived tissue rings for biomechanical analysis and tissue engineering. J. Vis. Exp., e3366.

Gwyther, T.A., Hu, J.Z., Christakis, A.G., Skorinko, J.K., Shaw, S.M., Billiar, K.L., and Rolle, M.W. (2011b). Engineered vascular tissue fabricated from aggregated smooth muscle cells. Cells Tissues Organs *194*, 13–24.

Karamariti, E., Margariti, A., Winkler, B., Wang, X., Hong, X., Baban, D., Ragoussis, J., Huang, Y., Han, J.D., Wong, M.M., et al. (2013). Smooth muscle cells differentiated from reprogrammed embryonic lung fibroblasts through DKK3 signaling are potent for tissue engineering of vascular grafts. Circ. Res. *112*, 1433–1443.

Kinnear, C., Chang, W.Y., Khattak, S., Hinek, A., Thompson, T., de Carvalho Rodrigues, D., Kennedy, K., Mahmut, N., Pasceri, P., Stanford, W.L., et al. (2013). Modeling and rescue of the vascular phenotype of Williams-Beuren syndrome in patient induced pluripotent stem cells. Stem Cells Transl. Med. *2*, 2–15.

Lee, T.H., Song, S.H., Kim, K.L., Yi, J.Y., Shin, G.H., Kim, J.Y., Kim, J., Han, Y.M., Lee, S.H., Shim, S.H., et al. (2009). Functional recapitulation of smooth muscle cells via induced pluripotent stem cells from human aortic smooth muscle cells. Circ. Res. *106*, 120–128.

Michel, J.B., Li, Z., and Lacolley, P. (2012). Smooth muscle cells and vascular diseases. Cardiovasc. Res. *95*, 135–137.

Niklason, L.E., Gao, J., Abbott, W.M., Hirschi, K.K., Houser, S., Marini, R., and Langer, R. (1999). Functional arteries grown in vitro. Science *284*, 489–493.

Patsch, C., Challet-Meylan, L., Thoma, E.C., Urich, E., Heckel, T., O'Sullivan, J.F., Grainger, S.J., Kapp, F.G., Sun, L., Christensen, K., et al. (2015). Generation of vascular endothelial and smooth muscle cells from human pluripotent stem cells. Nat. Cell Biol. *17*, 994–1003.

Rubin, L.L. (2008). Stem cells and drug discovery: the beginning of a new era? Cell *132*, 549–552.

Sundaram, S., One, J., Siewert, J., Teodosescu, S., Zhao, L., Dimitrievska, S., Qian, H., Huang, A.H., and Niklason, L. (2014). Tissue-engineered vascular grafts created from human induced pluripotent stem cells. Stem Cells Transl. Med. *3*, 1535–1543.

Tavernier, G., Mlody, B., Demeester, J., Adjaye, J., and De Smedt, S.C. (2013). Current methods for inducing pluripotency in somatic cells. Adv. Mater. *25*, 2765–2771.

Wang, C., Cen, L., Yin, S., Liu, Q., Liu, W., Cao, Y., and Cui, L. (2010). A small diameter elastic blood vessel wall prepared under pulsatile conditions from polyglycolic acid mesh and smooth muscle cells differentiated from adipose-derived stem cells. Biomaterials *31*, 621–630.

Wang, Y., Hu, J., Jiao, J., Liu, Z., Zhou, Z., Zhao, C., Chang, L.J., Chen, Y.E., Ma, P.X., and Yang, B. (2014). Engineering vascular tissue with functional smooth muscle cells derived from human iPS cells and nanofibrous scaffolds. Biomaterials *35*, 8960–8969.

Wanjare, M., Kuo, F., and Gerecht, S. (2013). Derivation and maturation of synthetic and contractile vascular smooth muscle cells from human pluripotent stem cells. Cardiovasc. Res. *97*, 321–330.

Xie, C.Q., Zhang, J., Villacorta, L., Cui, T., Huang, H., and Chen, Y.E. (2007). A highly efficient method to differentiate smooth muscle cells from human embryonic stem cells. Arterioscler. Thromb. Vasc. Biol. *27*, e311–e312.

Zaragoza, C., Gomez-Guerrero, C., Martin-Ventura, J.L., Blanco-Colio, L., Lavin, B., Mallavia, B., Tarin, C., Mas, S., Ortiz, A., and Egido, J. (2011). Animal models of cardiovascular diseases. J. Biomed. Biotechnol. *2011*, 497841.

Zeiger, A.S., Loe, F.C., Li, R., Raghunath, M., and Van Vliet, K.J. (2012). Macromolecular crowding directs extracellular matrix organization and mesenchymal stem cell behavior. PLoS One *7*, e37904.